



Svalbard ice-sheet decay after the Last Glacial Maximum: New insights from micropalaeontological and organic biomarker paleoceanographical reconstructions



A.S. Rigual-Hernández^{a,b,*}, E. Colmenero-Hidalgo^{a,c}, B. Martrat^d, M.A. Bárcena^a, A. de Vernal^e, F.J. Sierro^a, J.A. Flores^a, J.O. Grimalt^d, M. Henry^e, R.G. Lucchi^f

^a Área de Paleontología, Departamento de Geología, Universidad de Salamanca, 37008 Salamanca, Spain

^b Marine Research Centre, Department of Biological Sciences, Macquarie University, North Ryde, NSW 2109, Australia

^c Área de Geodinámica Externa, Facultad de CC, Biológicas y Ambientales, Universidad de León, Campus de Vegazana, s/n, 24071 León, Spain

^d Department of Environmental Chemistry, Institute of Environmental Assessment and Water Research (ID/EA), Spanish Council for Scientific Research (CSIC), Jordi Girona 18, 08034 Barcelona, Spain

^e GEOTOP, Université du Québec à Montréal, P.O. Box 8888, Montréal, Québec H3C 3P8, Canada

^f OGS (Istituto Nazionale di Oceanografia e di Geofisica Sperimentale), Borgo Grotta Gigante 42/c, I-34010 Sgonico, Trieste, Italy

ARTICLE INFO

Article history:

Received 31 January 2016

Received in revised form 21 October 2016

Accepted 23 October 2016

Available online 26 October 2016

Keywords:

Svalbard
Barents Sea
Deglaciation
Holocene
Microfossils
Dinocysts
Biomarkers

ABSTRACT

A marine sediment core retrieved from the middle continental slope of the northwestern Barents Sea was analyzed for its geochemical (alkenones) and micropalaeontological (diatoms, coccolithophores and dinocyst) content in order to reconstruct the evolution of upper ocean conditions and ice-sheet dynamics during the last 25 kyr. Additionally, quantitative reconstructions of sea surface conditions (temperature, salinity and sea-ice cover extent) were conducted based on the best analogue technique applied to dinocyst assemblages and on the alkenone unsaturation index. The sediment core contains a post Last Glacial Maximum depositional sequence unaffected by stratigraphic discontinuities. Low salinity and laminated sediments after 20 cal kyr BP, indicate a massive settling of meltwater sediment-laden plumes from the initial melting of the Svalbard-Barents Sea Ice Sheet on Western Svalbard. First record of measurable alkenones, together with a drop of the number of months of sea-ice cover and increase in SSTs suggests an intensification of the influx of Atlantic waters into the study area at ~15 cal kyr BP representing the termination of the last glacial period and onset of the Bølling interstadial. The first occurrence of diatoms and increase in the abundance of all microfossils marked the onset of the Holocene at 11.2 cal kyr BP when modern-type sea surface conditions were rapidly established in Western Svalbard. Reconstructions based on dinocyst data and alkenone unsaturation index suggest relatively warm and stable temperatures between 9.9 and 8.9 kyr BP and a decrease of SSTs from 4.2 cal kyr BP to present coinciding with the Holocene Thermal Maximum and the decrease of summer insolation in the high latitude northern hemisphere, respectively.

© 2016 Elsevier B.V. All rights reserved.

1. Introduction

The Atlantic meridional overturning circulation (AMOC) carries warm and saline Atlantic waters (AW) into high northern latitudes and returns cold deep waters southward towards the Equator. The inflow of warm and saline Atlantic waters across the Greenland-Scotland Ridge represents the major source of heat and salt to the Nordic Seas and Arctic Ocean (Aagaard et al., 1985), playing a pivotal role in the formation of the densest and deepest waters of the North Atlantic thermohaline circulation. The transport of heat by the North Atlantic Current

(NAC) flowing north to Fram Strait causes a dramatic reduction of the sea-ice extent via the warming of the intermediate water layers contributing to the fresh water input into the Greenland, Iceland and Norwegian Seas (Serreze et al., 2003; Seidov et al., 2015). Indeed, most evidence indicates that the inflow of Atlantic surface waters has played a key role in the growth and decay of ice sheets and climate changes in the Nordic Seas during the last deglaciation (Kristensen et al., 2013; Telesiński et al., 2015).

The front of the Svalbard-Barents Sea Ice Sheet on Western Svalbard (Fig. 1) underwent pronounced advances and retreats during the last glacial-interglacial cycle associated with fluctuations in the strength of the NAC flux (Martrat et al., 2003; Rasmussen et al., 2007; Jessen et al., 2010). The Storfjorden, in the southwestern Svalbard continental margin (Fig. 1), represented the western limit of this large ice sheet during

* Corresponding author at: Área de Paleontología, Departamento de Geología, Universidad de Salamanca, 37008 Salamanca, Spain.

E-mail address: andres.rigualhernandez@gmail.com (A.S. Rigual-Hernández).

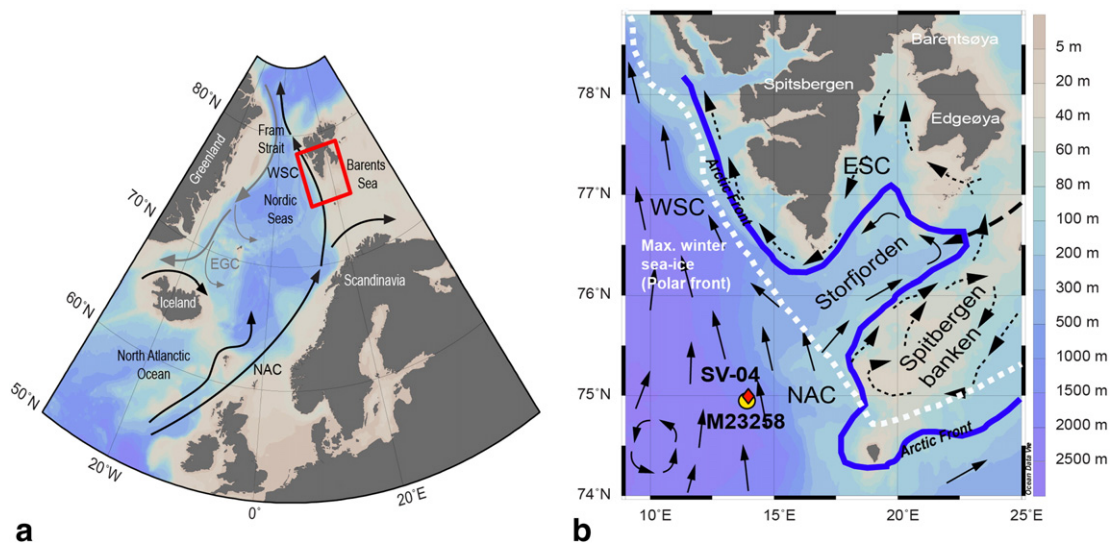


Fig. 1. (a) Map of the Nordic Seas and Barents Sea showing major surface currents. Red square highlights the study area. (b) Location of core SV-04 (red diamond) and M23258 (yellow circle) and trajectories of main oceanic surface currents after Loeng (1991) and Saloranta and Svendsen (2001). Abbreviations: NAC: North Atlantic Current; WSC: West Spitsbergen Current; ESC: East Spitsbergen Current; EGC: East Greenland Current.

the Last Glacial Maximum (LGM) and one of its main drainage pathways during the following deglaciation phase (see Ingólfsson and Landvik, 2013 for a review). Storfjorden is under the influence of both Atlantic and Arctic waters, and therefore, it is a highly sensitive area to global climate changes (Bauch and Weinelt, 1997; Landvik et al., 1998; Martrat et al., 2003; Rasmussen et al., 2007, among others). These characteristics make Storfjorden an ideal setting for studying the interactions between ice sheet dynamics, oceanography and climate (Jessen et al., 2010).

Analyses of the deep-sea sedimentary records of the Nordic Seas have provided important insights into the palaeoenvironmental and palaeoceanographic development of this region during the last glacial-interglacial cycle. Planktonic and benthic foraminifera (e.g. Bauch and Weinelt, 1997; Hald et al., 2004; Hald et al., 2007; Ślubowska-Woldengen et al., 2008; Andersson et al., 2010), coccoliths (e.g. Andrulleit and Baumann, 1998; Giraudeau et al., 2010; Dylmer et al., 2013), diatoms (Koç et al., 1993; Justwan and Koç, 2008; Berner et al., 2011; Hoff et al., 2016), dinocysts (e.g. Matthiessen and Baumann, 1997; Van Nieuwenhove et al., 2016) and a variety of chemical biomarkers (e.g. Martrat et al., 2003; Massé et al., 2008; Berben et al., 2014) have resulted particularly useful tools for the reconstruction of millennial-scale changes of the AMOC and the evolution of the ice-sheet dynamics in this climate sensitive area.

However, conclusions derived from these proxies often yield different results and magnitudes of the perceived climate variability in the region. This is most likely due to several biological, chemical and physical processes that complicate the interpretation of the sedimentary record. For example, the low species diversity and preservation issues of calcareous phyto- (e.g. coccolithophores) and zooplankton (e.g. foraminifera) often limit the interpretations on the fossil record (e.g. Solignac et al., 2008; Van Nieuwenhove et al., 2013). Moreover, silica dissolution of the diatom frustules in the water column and at the sediment-water interface largely alter the original diatom assemblages from their production in the surface layer until their eventual preservation in the fossil record (Ragueneau et al., 2000; Birks and Koç, 2002; Jordan and Stickley, 2010). In turn, dinoflagellate cysts have a proven potential for reconstructing surface ocean properties in the Nordic Seas and other cold oceanic regions. Due to their highly resistant organic walls, rich species diversity and good correlation with modern sea surface temperatures (SSTs), salinity (SSS) and

sea-ice cover, dinocysts have been proven as one of the most reliable proxies for the reconstruction of environmental conditions in the Nordic Seas (see Van Nieuwenhove et al., 2016 for a review).

In order to contribute to the understanding of the evolution of the Svalbard-Barents Sea Ice Sheet margin, an oceanographic expedition was conducted in the Storfjorden sedimentary system in August 2007 in the framework of the Spanish project SVAIS as part of the International Polar Year (IPY) Activity NICE STREAMS (Neogene ice streams and sedimentary processes on high-latitude continental margins). Detailed multibeam bathymetric survey, shallow seismic (TOPAS), single channel seismic reflection and coring of 6 sediment records in the slope and in the shelf were performed during the cruise. Onshore studies on the recovered dataset comprised measurement of palaeomagnetic and rock magnetic parameters, sedimentological, biogeochemical, isotopic and micropaleontological analyses, and 9 AMS radiocarbon datings (Pedrosa et al., 2011; Sagnotti et al., 2011; Lucchi et al., 2013; Llopart et al., 2015; Lucchi et al., 2015).

In this study we present a reconstruction of the sea-surface conditions in the Storfjorden area during the last deglaciation phase until present based on analyses performed in the piston core SV-04 recovered from the middle slope of the SW Svalbard continental margin (Fig. 1). SST, SSS, and seasonal duration of sea-ice cover have been quantitatively reconstructed by applying the Modern Analogue Technique (MAT) to dinocyst assemblages (e.g. de Vernal et al., 1993; Rochon et al., 1998; de Vernal and Hillaire-Marcel, 2000; de Vernal et al., 2005). Furthermore, changes in the abundance and the assemblage composition of diatoms, coccolithophores and dinocysts, together with alkenone concentration and alkenone derived SSTs, are presented and discussed to further document the paleoceanographical reconstructions.

2. Oceanographic setting

At present, the Storfjorden area is influenced by two distinct surface water masses. In the west, the Atlantic-sourced Western Spitsbergen Current (WSC) flows poleward along the continental slope carrying relatively warm and saline waters towards the Fram Strait and the Arctic Ocean (Rasmussen et al., 2007) (Fig. 1b). The WSC continues its flow into the Fram Strait as an intermediate water mass below the sea-ice covered Polar surface Water (Aagaard et al., 1987). On the Eastern Svalbard shelf, the cold and low saline Eastern Spitsbergen Current (ESC) flows from the Arctic Ocean towards the western coasts of Spitsbergen

along the eastern and southern margins of the archipelago. The large gradients of temperature and salinity between the two currents cause the development of the Arctic Front, that is distributed roughly parallel to the shelf break (Saloranta and Svendsen, 2001). The extent of the sea-ice cover determines the position of the Polar front, that in summer is located north of the Svalbard Archipelago (not showed in Fig. 1) and in winter coincides with the position of the Arctic front (Zamelczyk et al., 2012).

In winter, the area dominated by the WSC can be completely sea-ice-free while the ESC domains remain covered by sea ice; as a result, polynya on the inner shelf develop frequently, leading to formation of dense inner shelf water by brine formation (Skogseth et al., 2005). Present-day sea-ice cover in the study area, expressed here as number of months per year with >50% ice coverage, averages $0,32 \pm 0,69$ months/year (1953–2000 average from the National Snow and Ice Data Center – NSIDC). Modern SST and SSS in August are $7.56 \pm 1,39$ °C and $34.96 \pm 0,09\%$, respectively, while SST and SSS in February are 4.23 ± 0.92 °C and 35.04 ± 0.05 (World Ocean Atlas, 2001).

3. Materials and methods

3.1. Data set, age model and sediment facies

Six piston cores were recovered from the continental slope and shelf margin of the northwestern Barents Sea during the BIO Hespérides SVAIS cruise (29 July–17 August 2007). In this study we present the results from SVAIS core 04 (SV-04) retrieved in the middle slope area ($74^{\circ}57.425'N$, $13^{\circ}53.972'E$) at a water depth of 1839 m (Fig. 1). SV-04 is 310 cm long and contains a complete post LGM depositional sequence unaffected by stratigraphic discontinuities.

The sediment facies of core SV-04 were studied with CAT-scan radiographs, visual core logging, textural and compositional analyses including geochemical and XRF core scan analyses (Lucchi et al., 2013). The sedimentation rate was highly variable throughout core SV-04 (Fig. 2) with maximum values of up to 28 cm/ka between 79 and 187 cm (Fig. 2). The base of core SV-04 (310–262 cm) contained Mass Transport Deposits (MTDs), consisting of glaciogenic sediments (Fig. 3) incorporated locally older stratigraphic intervals (e.g. MIS 3 sediments at the base of SV-04 dating 25 cal kyr BP) (Fig. 3). Between 262 and 145 cm bsf, an

interval of IRD-rich and laminated sediments can be observed (Fig. 3). The uppermost part of the core was characterized by layered sediments between 145 and 60 cm, and by heavily bioturbated sediments between 60 and 0 cm (Lucchi et al., 2013).

The age model of SV-04 (Fig. 2) is based on 9 AMS (accelerator mass spectrometry) radiocarbon dates made on planktonic and benthonic foraminiferal tests, and high-resolution palaeomagnetic and rock magnetic parameters (Sagnotti et al., 2011; Lucchi et al., 2013). Raw AMS ^{14}C dates were obtained through the calibration software Calib 6.0 (Stuiver and Reimer, 1993), using the Marine09 calibration dataset (Reimer et al., 2009). Then an average marine regional reservoir effect $\Delta R = 84 \pm 23$ obtained from the Marine Reservoir Correction Database in Calib 6.0 for the north-western Barents sea area (south of Svalbard) was applied. Mean values for the calibrated age range of $\pm 1 \sigma$ were then normalized to calendar years (i.e. 1950 CE) and are here reported as cal yr BP.

The age model for the Holocene interval was refined using correlation of the tie-points to the closest regional stack curves of palaeosecular variation and relative geomagnetic paleointensity (Sagnotti et al., 2011). The age model of the sequence older than 10 ka was derived from correlations with the other cores recovered in the area (Lucchi et al., 2013) and the stacked MS-chronology of Jessen et al. (2010), considering a linear sedimentation rate between the dated/correlated horizons.

3.2. Microfossil analysis

A total of 31 samples taken at 10-cm interval were processed for diatom and coccolithophore analyses. Diatom sample processing and analyses were performed according to the standard randomly distributed microfossils method (Abrantes et al., 2005). Approximately 0.5 g of sediment was treated with hydrochloric acid (HCl) and hydrogen peroxide (H_2O_2) to remove carbonate and organic matter. Sediment was rinsed several times with bi-distilled water. Slides were mounted and diatom valves counted using a Leica DMLB compound light optical microscope at $1000\times$ magnification with phase-contrast illumination. The recommendations of Schrader and Gersonde (1978) were used as a basis for the counting of diatom valves. In brief, centric diatoms were counted as whole specimens if more than half of a valve was

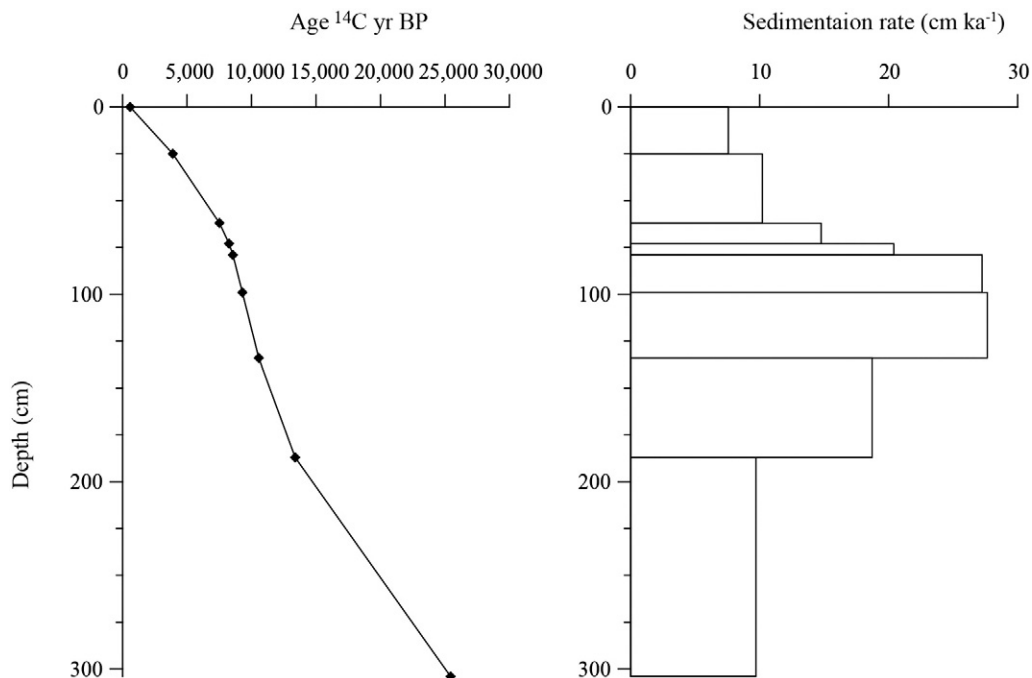


Fig. 2. Age-depth curve and sedimentation-rate histogram for piston core SV-04.

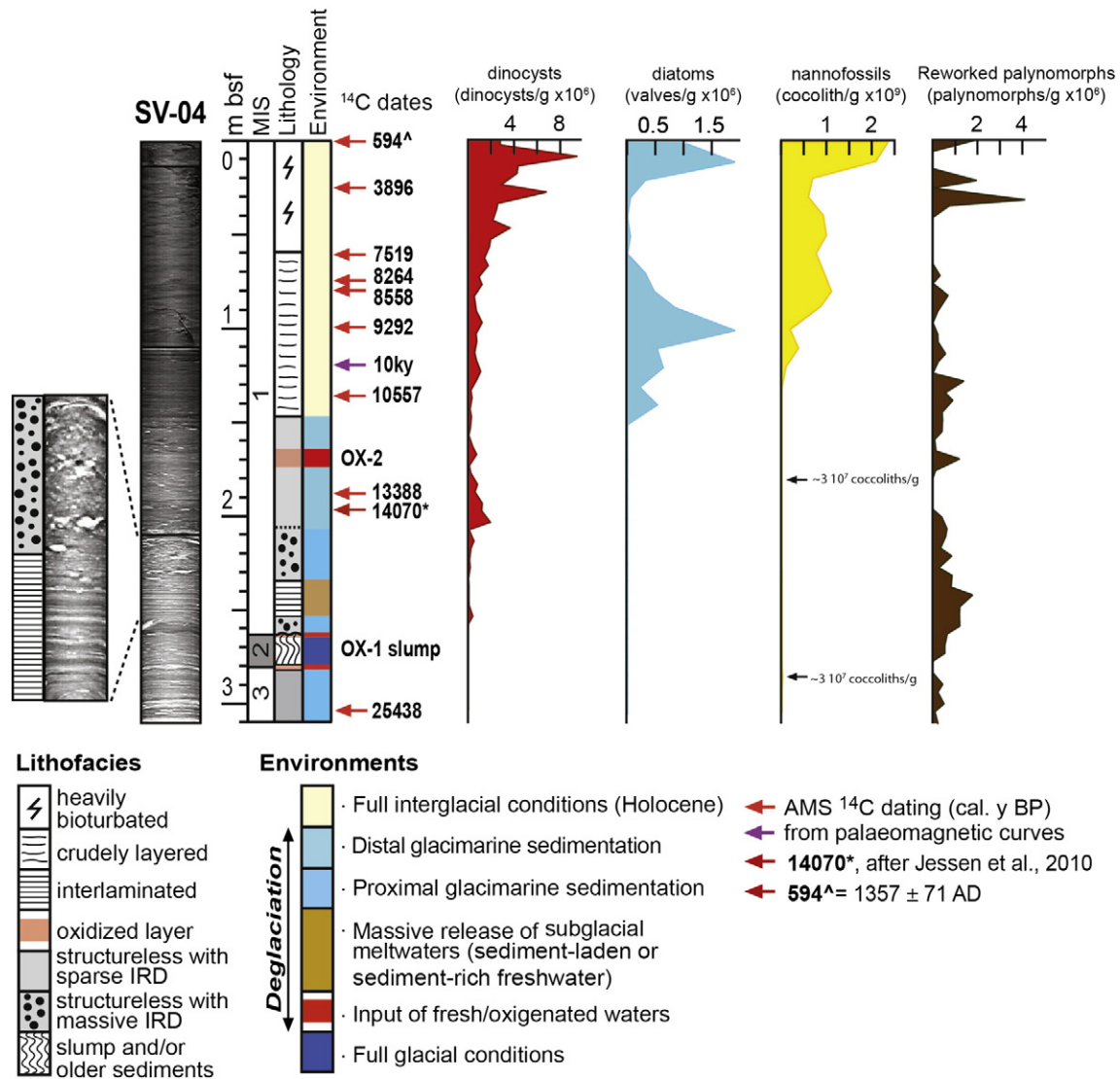


Fig. 3. X-ray photograph of core SV-04. Seismic units, marine isotopic stage (MIS), lithology, environmental interpretation, ¹⁴C dates (cal yr BP) and diatom, nannofossil, dinocyst and reworked palynomorph abundances plotted against depths and calibrated years BP. Lithological interpretation from Lucchi et al. (2013).

present (including the central area) while pennate diatoms were counted as half if only a single apical end was found on a valve. A minimum of 350 valves was counted for each sample when possible. All samples were assessed quantitatively for number of whole diatom valves per gram of dry sediment. Depending on diatom abundance, several traverses across each cover slip were examined. Samples were considered barren if no valves were found along at least five transects. Each diatom valve was identified to the lowest taxonomic level possible.

Samples for coccolithophore analysis were prepared following the methodology of Flores and Sierro (1997). A weighed amount of dry sediment was diluted in a volume of buffered water. A small fraction was extracted with a micropipette and dropped onto a Petri dish previously filled with more buffered water and with a cover slip in its bottom. After settling overnight the excess water was removed and the slide was left to dry and then mounted using Canada balsam. Coccoliths were identified and counted using a LEICA DMRXE polarized light microscope at 1250× magnification. At least 300 individuals were counted in each sample when possible. Samples were considered barren if no coccoliths were found in at least 30 randomly selected fields of view. Coccolith abundance per gram of sediment was obtained using the method described in Flores and Sierro (1997).

Palynological analyses were made at a 4–6 cm sampling interval for a total of 60 samples. Preparation of the palynological samples followed

the standardized procedure of GEOTOP (de Vernal et al., 1996a), according to which 5 g of wet sediment were sieved at 10 and 106 μm and treated several times with HCl and hydrofluoric acid (HF) to dissolve carbonate and silica particles, respectively. The remaining residue was mounted on an optical slide using glycerin gel for observation in transmitted light microscopy at 400× to 1000× magnification. A minimum of 300 dinoflagellate cysts were identified and counted in most samples, except for the lower part of the core where the palynomorph content was very sparse. Spores, pollen grains and benthonic foraminiferal organic linings and reworked palynomorphs were also counted, although only reworked palynomorphs are presented in this study and used as tracers of allochthonous inputs of surrounding outcrops. Absolute abundance of palynomorphs (cyst/gram dry sediment) was calculated following the marker-grain method (Matthews, 1969) that provides results with an accuracy of ± 10% for a 0.95 confidence interval (de Vernal et al., 1987).

3.3. Quantitative sea-surface estimates based on dinocyst assemblages

Dinoflagellate cysts (dinocysts) mainly relate to the primary production occurring in the photic zone (e.g. Taylor, 1987). The distribution of dinocyst assemblages in high latitude environments permits us to apply the modern analogue technique (MAT; e.g. Guiot and de Vernal, 2011)

for the quantitative reconstruction of sea-surface parameters including salinity, maximum and minimum annual sea surface temperature and the seasonal extent of sea-ice cover, which is expressed in number of months per year with >50% sea-ice coverage (de Vernal et al., 1996b; de Vernal et al., 1997; Rochon et al., 1998). The MAT applied to the dinocyst assemblages has been shown to be one of the most useful methods for the reconstruction of past sea-surface conditions over the northern North Atlantic (de Vernal et al., 2000; Guiot and de Vernal, 2011). Here, we have used the updated reference dinocyst database that includes 1492 sites from mid-high latitudes of the Northern Hemisphere and 64 taxa (cf. de Vernal et al., 2013). The reconstructions were made from the search of the 5 best modern analogues after log transformation of the taxa percentages. Validation exercises yield error of prediction of ± 1.8 and ± 1.3 °C for August and February SSTs respectively, ± 2.3 psu for salinity, and ± 1.4 months/year of sea-ice cover (de Vernal et al., 2000).

3.4. Lipid biomarker analysis

Centrifuge tubes and test tubes used for the analyses were heated overnight at 400 °C after cleaning by sonication for 15 min with alkaline detergent at 5% (Extran AP13, Merck Darmstadt, Germany). Solvents with quality for organic trace analysis (dichloromethane, hexane, methanol, toluene) and reagents (KOH, bis-(trimethylsilyl)trifluoroacetamide-BSTFA-) were purchased from Merck (Darmstadt, Germany).

The concentration of the heptatriaconta-8E,15E,22E,29E-tetraen-2-one (C₃₇:4Me), heptatriaconta-8E,15E,22E-trie2-one (C₃₇:3Me) and heptatriaconta-15E,22E-die2-one (C₃₇:2Me) was determined using n-hexatriacontane as internal standard.

Sediment samples were freeze-dried (12 h). The amount of dry sediment for analysis was up to 2.5 g. Ultrasound-assisted extraction and vortex shaking were done using 7.5 mL of dichloromethane (15 min repeated three times, ensuring an extraction higher than 90%). The extracts were dried under nitrogen and hydrolysed with 7% potassium hydroxide in methanol to avoid interferences in detection and quantification of the compounds (2 mL; 12 h; room temperature). Extraction with hexane (2 mL; three times) yielded a fraction enriched in neutral compounds, which was cleaned with ultra-pure water. The purified extracts were derivatized with BSTFA (12 h; room temperature). Samples were injected diluted in toluene. They were analyzed with a Varian gas chromatograph Model 450 equipped with a 1079 Programmable Temperature Vaporizing (PTV) Injector for cold on-column (sample volume 1 µL, fast injection rate) and a Flame Ionization Detector (GC-FID; ceramic flame tip; temperature 320 °C, range 12). The instrument was equipped with a CPSIL-5 CB column coated with 100% dimethylsiloxane; film thickness of 0.12 µm; L (m) * ID (mm) * OD (mm): 50 * 0.32 * 0.45. Hydrogen was the carrier gas (2.5 mL/min). Oven temperature was programmed from 90° (holding time of 1 min) to 170 °C at 20 °C/min, then to 280 °C at 6 °C/min (holding time 25 min), and finally, to 315 °C at 10 °C/min (holding time of 12 min). The injector was programmed from 90 °C (holding time of 0.5 min) to 310 °C at 200 °C/min (final holding time was 55 min). The acquisition program used for this analysis was the Thermo Atlas. Absolute concentration errors were below 10% (LoD 0.2 ppm; LoQ 0.4 ppm). The resolution between the heptatriaconta-8E,15E,22E-trie2-one and heptatriaconta-15E,22E-die2-one ranged between 1.5 and 1.7. Reproducibility tests showed that the uncertainty in the U^K₃₇ determinations [$U^K_{37} = (C_{37:2Me} - C_{37:4Me}) / (C_{37:2Me} + C_{37:3Me} + C_{37:4Me})$; U – unsaturation, K – ketone and 37 – ketone chain length; Brassell et al., 1986] was lower than 0.0165 (ca. 0.5 °C). The calibration used is specific for the Nordic seas ($U^K_{37} = 0.029 * SST + 0.162$, $r^2 = 0.98$; $n = 109$; Rosell-Melé et al., 1995) where substantial proportions of the C₃₇:4Me homolog are to be found (Rosell-Melé et al., 2002). Selected samples were fractioned by using an Agilent 1100 series for evaluation of coelutions and final confirmation of compound identification.

4. Results

4.1. Microfossil assemblages

The absolute abundance of dinocysts, diatoms and coccoliths record pronounced changes with coherent fluctuations throughout core SV-04 (Fig. 3). Maximum microfossil abundances characterize the Holocene (up to $9.4 \cdot 10^4$ cysts/g, $1.89 \cdot 10^6$ valves/g and $2.3 \cdot 10^9$ coccoliths/g, respectively). In contrast, the interval prior to 11.2 cal kyr BP is barren of diatoms and contains low dinocyst and coccolith numbers (down to 86 cysts/g and $0.3 \cdot 10^8$ coccoliths/g, respectively) (Fig. 3). The low microfossil abundance in some samples of SV-04 (mainly from the lower most section of the core) only allowed for low dinocyst, diatom valve and coccolith counts (<50) and the consequent “loss” of low-abundance species (Fátela and Taborda, 2003), that are often characterized by more narrow ecological constraints. Thus, interpretations based on the microfossil assemblages from these samples should be made with caution. Samples with low counts are highlighted in Fig. 4 (see Figure caption for details).

The relative abundance of dinocyst taxa from core SV-04 is shown in Fig. 4. The most abundant taxa are *Brigantedinium* spp., *Operculodinium centrocarpum*, *Spiniferites elongatus* and *Nematosphaeropsis labyrinthus*, which represent together about 90% of the assemblage. *Brigantedinium* spp. is the most abundant taxon in the lowermost part of the core (up to 87%) and exhibits a gradual decline upwards. The cosmopolitan taxon *O. centrocarpum* shows an opposite pattern, representing up to 94.5% of the dinocyst assemblage in the most recent sample of the core (Fig. 4). Maximum percentage of *S. elongatus* is registered between ~15 cal kyr BP and ~11.5 cal kyr BP, just before the beginning of the Holocene, while *N. labyrinthus* shows its maximum relative abundance afterwards, from ~11.2 to ~6.7 cal kyr BP. Reworked palynomorphs of pre-Quaternary age occur in low number throughout the core (<100 palynomorphs/g) although slightly higher values are registered between 20.1 and 18 cal kyr BP, at 12.3 cal kyr BP and during the early and late Holocene (Fig. 3).

The first diatom occurrence in core SV-04 coincides with the onset of the Holocene (Fig. 3). Diatom abundance shows two distinct maxima, centered at ~9.3 and ~1.5 cal kyr BP. The first peak is mainly composed by *Coscinodiscus* spp. (up to 75%) and shows high abundances of *Rhizosolenia* spp. and *Paralia sulcata*, whereas the most recent maxima is dominated by *Chaetoceros* Resting Spores (RS) (up to 72%) (Fig. 4).

Coccolithophores are relatively abundant in the Holocene sediment, peaking at ~8.9 cal kyr BP and in the top centimetres of the record. In the lower half of the core most samples are barren of coccoliths except during 2 short intervals centered at ~12.9 and 23.4 cal kyr BP. In all samples, the assemblages are dominated by *Emiliania huxleyi* (<4 µm) and *Coccolithus pelagicus*, with minor amounts of *E. huxleyi* (>4 µm), “small” *Gephyrocapsa* and *Gephyrocapsa muelleriae*. During the Holocene, at ca. 8.0 cal yr BP, there is a shift of the assemblage dominated by *E. huxleyi*/*G. muelleriae* to an assemblage dominated by *C. pelagicus*.

4.2. Reconstructions of sea-surface conditions

Sea surface conditions for the six samples with <50 dinocysts in the lowermost part of the core (Fig. 4) were not estimated in order to avoid artifacts caused by the low counts. These reconstructions of sea-surface conditions based on dinocysts assemblages are compared with the SST derived from alkenones in SV-04 and the nearby core M23258 (Martrat et al., 2003) which data is also presented in Fig. 5 to support our interpretations.

The reconstructions of sea-surface conditions based on dinocysts assemblages suggest large amplitude variations in the last deglaciation period, until about 11.5 cal kyr. BP (Fig. 5). At the beginning of the Holocene, the results suggest that similar conditions to present were established and remained relatively stable with SST of about 5 and 8.5 °C in February and August, respectively. The alkenone-based SSTs

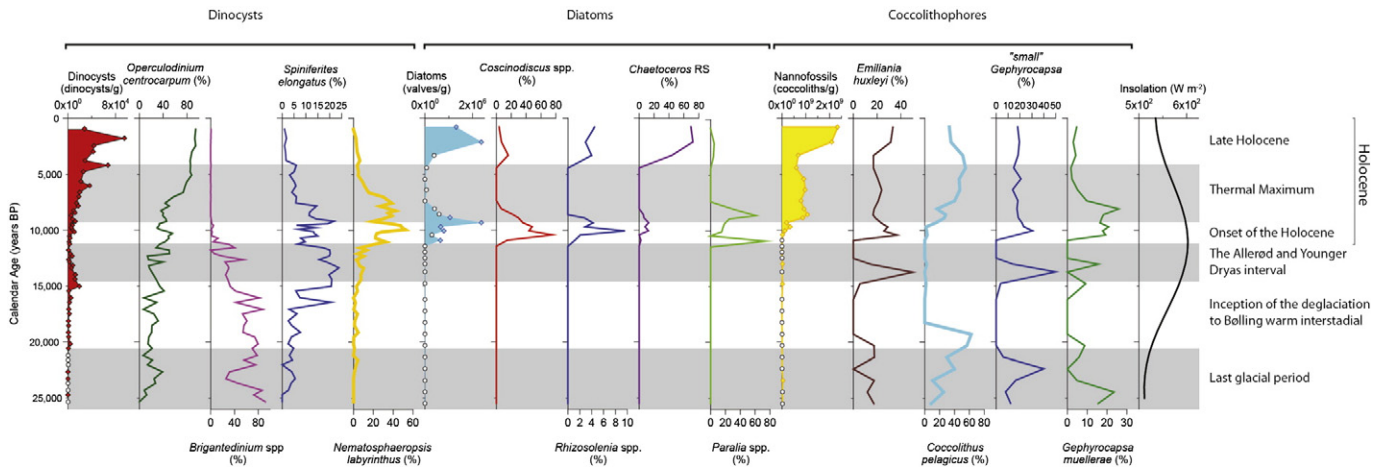


Fig. 4. Down-core profile of the relative abundance of the main dinocyst, diatom and coccolithophore taxa in the piston core SV-04. Samples with >50 individuals counted are represented by diamonds while samples with <50 individuals are represented by white circles. Summer insolation curve at 75° for the studied interval following Laskar et al. (2004) is also shown.

at SV-04 suggest relatively warm and stable annual SSTs (ranging between 6 and 7 °C) from 8.2 to 4.2 kyr BP followed by a stepwise cooling during middle and late Holocene (down to 4 °C) (Fig. 5).

Total C₃₇ alkenones are synthesized by some haptophyte microalgae, mainly coccolithophorids. Since these compounds are relative resistant to degradative processes, they are often used to trace changes in marine productivity over time (e.g. Villanueva et al., 1998; Martrat et al., 2003). Both SV-04 and M23258 show similar downcore variations of total C₃₇ alkenone content, with peak values at ~10 kyr BP, followed by a gradual decrease until ~5 yr BP and a final increase of alkenone content until present.

5. Discussion

The analysis of core SV-04 revealed large sedimentological, biogeochemical and microfossil assemblage changes that reflect variations in the oceanographic circulation and glacial dynamics of Storfjorden, especially during the late glacial and deglaciation. Based on the most

important changes in the sedimentological and microfossil assemblage together with comparisons with previous studies in the Western Svalbard region, four intervals were differentiated: the last glacial (>20.6 cal kyr BP), the inception of deglaciation and Bølling warm interstadial (20.6–14.6 cal kyr BP), the Allerød and Younger Dryas interval (15–11.2 cal kyr BP), and the Holocene (11.2 cal kyr BP to present).

5.1. Last glacial period (>20.6 cal kyr BP)

Lack of radiometric data between 25 and 14 kyr due to low abundance of planktonic foraminifera precluded accurate dating of the deposits below 200 cm of SV-04 (Fig. 2). However, the combined analysis of the sedimentology and the microfossil assemblages provides some insights into the evolution of the upper ocean conditions and ice-sheet dynamics of Western Svalbard during this interval. The mass-transported sediments observed in the lowermost part of core SV-04 (i.e. below 256 cm bsf, Fig. 3) correspond to consolidated debris flows derived from the down-slope transport of glacial sediments, which

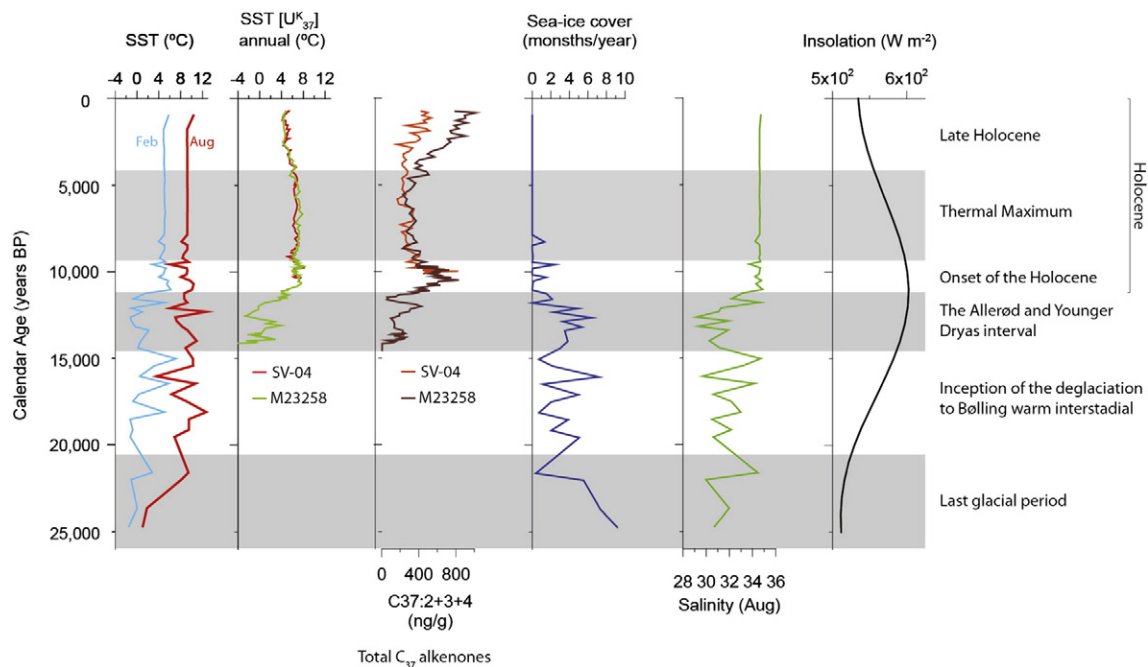


Fig. 5. Down-core profiles of estimated sea surface conditions derived from dinocyst assemblages (temperature, salinity and sea-ice cover), sea surface temperatures derived from alkenones and total C₃₇ alkenones in the piston core SV-04 and core M23258 after Martrat et al. (2003). Note that for dinocyst based reconstructions the lines represent the most probable value of a set of five best analogues in the reference database. The summer insolation curve at 75° for this interval following Laskar et al. (2004) is also shown.

are characteristic of glacial deposition in Trough Mouth Fan (TMF) systems of the Barents Sea (e.g. Laberg and Vorren, 1995; Andersen et al., 1996; Rasmussen et al., 2007; Lucchi et al., 2015). These debris flows most likely settled when the Svalbard-Barents Sea Ice Sheet front reached its maximum extent at the Last Glacial Maximum (ca. 21 ka) (Landvik et al., 1998; Ottesen et al., 2005; Jessen et al., 2010; Lucchi et al., 2015). Simultaneously, low temperatures and extensive ice cover were common above SV-04 during this interval (Fig. 5), causing harsh environmental conditions for the occurrence of coccoliths and the absence of diatoms in the sediments suggests that phytoplankton growth around SV-04 location was limited during this interval. Moreover, from 303 to 203 cm bsf dinocyst assemblages were largely dominated by *Brigantedinium* spp., an opportunistic heterotrophic taxon that can gain advantage over phototrophs under low light conditions such as arctic sea ice (Rochon et al., 1999; Van Nieuwenhove et al., 2016). Sea surface reconstructions based on dinocyst assemblages suggest maximum sea ice cover conditions for this interval, but with a significant reduction of the number of months of sea ice cover and salinity coupled with an increase in summer SSTs at ~22 cal kyr (Fig. 5), reaching values similar to those shown during the Holocene. Although we urge caution in the exact chronology of this event observed in our records due to poor constrains of the SV-04 age model for this interval, our data suggests that warming was probably accompanied by an increase in the productivity in the upper photic zone as shown by the dominance of dinocyst and coccolithophore assemblages by cosmopolitan taxon such as *O. centrocarpum* and the “small” *Gephyrocapsa* group (Fig. 4). Such short-term warming events during the LGM to Heinrich event 2 interval are often reported in records further downstream the NAC path (Knutz et al., 2007; Hall et al., 2011). In addition, the increase in SST differences between summer and winter values can be interpreted as increased seasonal temperature contrast in the area due to the increase in insolation from ~23 cal kyr onwards.

5.2. Inception of the deglaciation to Bølling warm interstadial (20.6–14.6 cal kyr BP)

The onset of the deglaciation is marked by a strong seasonal SST contrast, decreasing salinities and increasing sea-ice cover (Fig. 5) coupled with the deposition of a layer of oxidized sediments (Fig. 3) that is related to the release and sink of oxygenated, fresh and cold waters from the initial melting of the Svalbard-Barents Sea Ice Sheet. The presence of this oxidized layer is consistent with the start of the glacial retreat that was dated at $20,000 \pm 500$ cal yr BP by Jessen et al. (2010) and Lucchi et al. (2015). Indeed, it is likely that the oxidized layer (OX-1) represents the record of the first abrupt global sea-level rise after the LGM caused by the intense melting of the northern hemisphere mountain glaciers and ice sheets, the so-called Meltwater Pulse 19 ka (MWP-19 ka) (Clark et al., 2002b; Clark et al., 2004; Lucchi et al., 2015). This hypothesis is consistent with our reconstructions (i.e. sharp decrease of SSTs and SSS associated to fresh water input, Fig. 5) and with those of Lucchi et al. (2015) who reported enhanced ventilation of the deep ocean with possible seasonal sea-ice surface conditions along the NW Barents Sea continental margin. This scenario with relatively extended sea ice and low salinities characterized most of this interval, and was the probable cause of the low phytoplankton production in the area (Fig. 4). Only dinocysts are present in significant numbers and their assemblages are dominated by *Brigantedinium* spp., thus supporting possible low light conditions in the photic zone that most likely hampered coccolithophore and diatom growth. Sedimentation most likely took place in a few hundred years by the massive settling of meltwater sediment-laden plumes (*plumites*) from the ice stream grounded at or near the shelf edge (Lucchi et al., 2013) causing the deposition of a laminated sequence (Fig. 3). A peak of reworked palynomorphs during this interval is consistent with a high discharge of meltwater and terrigenous sediments (Fig. 3). This is further supported by the dominance of reworked organic matter strongly modified by microbial alteration in

nearby core M23258 (Martrat et al., 2003), with a composition consistent with ice-rafted debris from the Spitsbergenbanken accumulated on the continental slope (Bischof, 1994). Despite the fact that the low abundance of planktonic foraminifera precluded the accurate dating of this interval, reliable correlations can be made with equivalent postglacial deposits described along the West Svalbard continental slope and outer shelf in neighboring glacial TMF systems dating 14.7–14.4 cal ka BP (Elverhøi et al., 1995; Rasmussen et al., 2007; Jessen et al., 2010; Rütther et al., 2012; Carbonara et al., 2016). Lucchi et al. (2015) proposed that this massive meltwater event registered in the sediments of the Storfjorden most likely represents the Meltwater Pulse 1A (MWP-1A) of Fairbanks (1989). MWP-1A represented one of the most pronounced ice melting events of the last deglaciation responsible for an exceedingly rapid sea level rise of about 20 m within a few hundred years (Fairbanks, 1989; Clark et al., 2002a; Rinterknecht et al., 2006; Deschamps et al., 2012). According to Deschamps et al. (2012), the MWP-1A is coeval with the Bølling warming (14.65–14.31 cal kyr BP) resulting from a strengthening of the Atlantic meridional overturning circulation promoting heat transport from low to high-latitude regions (Kienast et al., 2003; Weaver et al., 2003; Liu et al., 2009). Sea surface reconstructions clearly indicate that, as for the previous Meltwater Pulse (19 ka), also in this case the freshening and cooling of surface waters by extensive glacial melting, lead to a progressive increase of sea-ice cover (from 2 to 4 months/year) as consequence of strong stratification of the water column with surface fresh/brackish waters having lower freezing point. The combination of cold meltwater and extended seasonal sea-ice coverage determined harsher environmental conditions as indicated by the inversion trend of the SST curve possibly marking the Old (or Older) Dryas. According to Lucchi et al. (2015) the thick massive IRD interval topping the laminated sediments was produced by a major ice sheet collapse at the end, or during, the MWP-1A that was coupled with an increase of the biological activity in the area.

5.3. The Allerød and Younger Dryas interval (14.6–11.2 cal kyr BP)

The onset of the Bølling/MWP-1A event at 14.6 cal kyr BP triggered the irreversible and fast decay of the ice-sheet that never developed again to LGM reaches during any of the subsequent cold stadials. The gradually increasing influence of warm Atlantic waters over the sedimentation is reflected by the shift of the sediment facies to bioturbated sediments containing rare IRD (Fig. 3) and progressive reduction of seasonal duration of the sea-ice cover as estimated from the dinocyst-based reconstruction (Fig. 5). The transition towards milder conditions in the Svalbard continental margin was accompanied with a small increase in marine productivity as reflected by the increase in the dinocyst abundance, and by the first occurrence of measurable alkenone concentration in the nearby M23258 site at ca. 13.9 cal kyr BP (Fig. 5b; Martrat et al., 2003). Despite of a clearly higher marine component to the sedimentation, this period is still principally characterized by the of high amount of organic matter of continental origin such as C₂₃–C₃₃ odd carbon numbered n-alkanes and C₂₂–C₂₈ even carbon numbered n-alkan-1-ols (Martrat et al., 2003). This is in agreement with previous studies from the Svalbard region (Mangerud et al., 1998; Nørgaard-Pedersen et al., 2003; Jessen et al., 2010) and suggests a close interplay between a renovated warm Atlantic current in the continental margin of Storfjorden and the melting ice sheet.

The layer of oxidized sediments (OX-2; Fig. 3) registered between 12.6 and 12.1 cal kyr BP occurred during the Younger Dryas stadial (12.9–11.7 kyr BP; Rasmussen et al., 2006; Broecker et al., 2010; Martrat et al., 2014). There is evidence of a retreat of the Barents Sea ice sheet into the Barents Sea shelf and fjords during this interval that most likely resulted in the opening of a sea ice free corridor south of Svalbard, allowing the East Spitsbergen Current to flow through towards the northernmost Atlantic area (Rasmussen et al., 2007). The dinocyst-based reconstruction of sea surface conditions during the Younger Dryas interval suggests low winter temperatures (down to

–1 °C), low salinities (~29) and sea-ice cover for up to six months per year (Fig. 5). Such conditions would account for the very low productivity suggested by the low abundance of microfossils during this interval and are consistent with the hypothesis of enhanced inflow of the cold East Spitsbergen Current promoting harsher environmental conditions. Interestingly, during most of the Bølling-Allerød and Younger Dryas interval dinocyst MAT-SSTs records show a strong seasonal gradient of up to 10 °C between summer and winter. This strong seasonality is likely to have been caused by increasing summer insolation and CO₂ levels that characterized the late deglacial period (Buiertz et al., 2014).

The end of the deglaciation is marked by increasing winter SSTs, which most likely caused the progressive decay of sea ice cover in the area and the gradual increase of SSS (Fig. 5). The reconstruction of sea surface conditions during this interval is consistent with the deposition of the layer of bioturbated sediments with rare IRDs (Fig. 3), which were most likely generated by ice-rafting pulses from the retreating calving line of the inner shelves of Svalbard and the Barents Sea (Andersen et al., 1996; Mangerud et al., 1998; Jessen et al., 2010). This layer is also observed in the organic matter composition in the form of an increase of reworked microbial n-alkanes characteristic of ice-rafted debris (Martrat et al., 2003).

5.4. Holocene (11.2 cal kyr BP to present)

The onset of the Holocene at ca. 11.2 cal kyr BP is marked by the first occurrence of diatoms and by a rapid increase in the abundance of all microfossils (Fig. 4), suggesting favorable conditions for algal production and preservation along the western Svalbard continental slope. This idea is supported by the peak abundances of *Paralia sulcata*, a brackish to marine diatom species that is often associated with nutrient rich waters and coastal upwelling (McQuoid and Nordberg, 2003; Di et al., 2013). Sea-surface reconstructions based on both dinocyst assemblages and alkenones indicate that modern-type environmental conditions, with little, if any, seasonal sea-ice development were rapidly established at the beginning of the Holocene (Fig. 5). The microfossil assemblages and quantitative reconstruction of sea-surface conditions strongly suggest the dominant influence of Atlantic waters along the Norwegian margin from the beginning of the Holocene. The onset of the Holocene is accompanied by contour-current-related deposition (Fig. 3) indicating a change in the dominant sedimentary processes on the lower slope of Storfjorden from down-slope mass wasting sedimentation to along-slope current-controlled deposition (Lucchi et al., 2013). Peak solar insolation at 75°N during this interval most likely contributed to the reduction of the sea-ice cover in the western Barents shelf (Sarnthein et al., 2003; Łącka et al., 2015). Sea-ice cover decrease resulted in the increased accumulation of solar energy by the ocean, a process that accelerated the retreat of the ice sheets towards the fjords heads (Baeten et al., 2010; Jessen et al., 2010; Łącka et al., 2015).

Maximum accumulation of diatoms registered between 9.9 and 8.9 cal kyr BP seems to result from the positive response of this phytoplankton group to the maximum insolation anomaly in the northern hemisphere occurred between 10 and 9 kyr BP, i.e. the Holocene Thermal Maximum (Figs. 4 and 5; Koç et al., 1993; Kaufman et al., 2004; Renssen et al., 2009; Renssen et al., 2012). The significant relative contribution of *E. huxleyi* (<4 µm), “small” *Gephyrocapsa* and *G. muelleriae* to the coccolith assemblages during this interval also suggest a strong inflow of warm Atlantic waters into the study area and the northern and/or western displacement of the Arctic front (Stabell, 1986; Koç et al., 1993; Baumann et al., 2000). Moreover, malacological assemblages along the Svalbard shoreline indicate an increase of the sea-surface temperatures during this period, which is marked by the occurrence of thermophilous mollusc shells from 9.5 kyr (Salvigsen et al., 1992). The large relative contribution of “shade flora” diatoms *Coscinodiscus* and *Rhizosolenia* (Kemp et al., 2000; Kemp and Villareal, 2013) during this interval may reflect a shallowing of the summer mixed layer due to the stronger insolation and melting of the ice rafted from the glaciers

that could have facilitated the formation of a deep chlorophyll maximum during summer-autumn. Deterioration of the water column stability during the summer-autumn transition could potentially lead to mass mortality and sinking of these diatom species facilitating their preservation in the sediments (Kemp et al., 2000; Maddison et al., 2006). A similar maximum in the relative contribution of *Coscinodiscus* and *Rhizosolenia* species have also been reported south of the study location, in the middle slope of the Kveithola Trough Mouth Fan by Carbonara et al. (2016). The former authors linked the increase in the abundance of these species to a pronounced inflow of Atlantic waters and shallowing of the mixed layer. These results are consistent with reported data on potential water density from dinoflagellate cyst assemblages and δ¹⁸O of *Neogloboquadrina pachyderma* (s), indicating that from the early Holocene to about 6.5 ka B.P. relatively light (i.e. δ¹⁸O depleted) surface waters occupied the western Nordic Seas (Van Nieuwenhove et al., 2016).

Three short-lived episodes of cooling marked with lower SSTs and sea-ice cover spreading (up to 2.4 months/year) are recorded at approximately 10.3, 9.6 and 8.2 cal kyr BP during the early Holocene (Fig. 5). This stepwise transition from the Younger Dryas to the mild conditions of the Holocene has been documented in other records from the Nordic Seas (e.g. Fig. 5) and has often referred to as the Pre-Boreal Oscillation (Martrat et al., 2003; Sarnthein et al., 2003; Rasmussen et al., 2007). The last cold spell at 8.26 cal kyr BP correlates in time with the Bond event number 5 (8.2 cal kyr BP; Bond et al., 1997) which is considered as the most prominent Holocene climatic event in the Greenland ice cores (Alley et al., 1997). The so-called “8.2 kyr event” has been hypothetically linked to a disruption of North Atlantic Deep Water formation related to a catastrophic release of freshwater from the glacial lakes Agassiz and Ojibway through the Hudson Strait when the residual dome of the Laurentide Ice Sheet collapsed (Klitgaard-Kristensen et al., 1998; Barber et al., 1999; Stroup et al., 2013 and references therein). However, the signal in surface waters of the Labrador Sea and northwest North Atlantic is barely distinguishable (Hillaire-Marcel et al., 2007) and high resolution modeling experiments of ocean circulation do not support the hypothesis of the Atlantic meridional overturning collapse triggered by the glacial lake Agassiz discharge (Condon and Winsor, 2011).

Reconstructions based on U^K₃₇ index at both SV-04 and the nearby M23258 suggest very similar SST trends during the Holocene with relatively warm and stable annual SSTs (ranging between 6 and 7 °C) from 8.2 to 4.2 kyr BP followed by a stepwise cooling during middle and late Holocene (down to 4 °C) (Fig. 5). Interestingly, dinocyst MAT-SSTs suggest stable conditions throughout the whole Holocene with winter and summer temperatures of 4–6 °C and 7–10 °C, respectively (Fig. 5). It should be noted that despite the fact that both proxies exhibit different trends, their overall variation range for the whole Holocene is coherent taking into consideration the following aspects: (1) the reconstructed SSTs during the Holocene suggest small amplitude changes for both proxies and variations are within the range of accuracy of the approaches, i.e. ± 1.3 and ± 1.8 °C for the winter and summer SSTs in the case of dinocysts (de Vernal et al., 2000) and ± 0.5 °C in the case of alkenones (Martrat et al., 2003); (2) U^K₃₇ index represents an annual SST estimate, although probably seasonally biased towards the time of coccolithophore production (i.e. late summer and autumn in the Nordic Seas; Andruleit, 1997); (3) whereas MAT applied to dinocysts permits to distinguish between winter and summer SSTs, and thus averaging these values yields temperatures of ~5–8 °C, a SST range very similar to that suggested by the alkenones.

The lack of high SST in dinocyst MAT-SSTs during the Thermal maximum compared to alkenone-based records seems, however, somewhat contradictory. Several factors may account for the different trends suggested by the two proxies during this interval. Cortese et al. (2005) and Hald et al. (2007) attributed the absence of high SSTs during the early Holocene in planktic foraminifera MAT-SSTs, compared to diatom and alkenone records to different water column habitats of the analyzed microplankton groups. However, this hypothesis seems unlikely in our

case as the bulk biomass of both dinoflagellates and calcareous nannoplankton are generally considered to live associated to the surface layer. Another possible cause for discrepancies between proxies could be due to the fact that coccolithophores are rather stenohaline, and therefore, any change in salinity by fresh water input from sea ice melt might have an impact on their biomarker signature, and consequently in the U^{K}_{37} index. A last possibility might be the selective transport of the light alkenone molecules produced further south and advected to the study area by Atlantic waters, while the heavier dinoflagellate cysts most likely were produced and exported in situ, therefore reflecting environmental conditions of two different systems. Unfortunately, none of these hypotheses can be assessed with the current data sets.

The warmer temperatures suggested by the alkenone records (Fig. 5) during 8.2 to 4.2 kyr BP broadly corresponds to the Thermal Maximum (i.e. an unusually warm period from about 9000 to 6000 years BP registered in many palaeoclimatic records in high northern latitudes) that has been previously constrained in the Svalbard region between 8.8 and 5.0 kyr BP (Hjort et al., 1995; Andersen et al., 2004). The origin of this thermal maximum is thought to be primarily driven by orbital forcing, but changes in the strength of the North Atlantic Current could also be invoked as an important mechanism (Jansen et al., 2009). The increase in the total coccolith abundance during this interval suggests enhanced primary productivity conditions. This is somewhat at odds with the drop in the total diatom abundance until 4 kyr BP (Fig. 4). It is possible that diatom production during this interval was also high stimulated by the Climate Optimum conditions but dominated by bloom-forming and weakly silicified species that often dominate high productive systems. These bloom-forming diatoms tend to rapidly dissolve in the water column and sediment water-interface, and therefore, are often not preserved in the sedimentary record (Assmy et al., 2013; Rigual-Hernández et al., 2016).

From ca. 4.2 cal kyr BP diatom, coccoliths, dinocyst and alkenone concentrations exhibit a pronounced increase reaching maximum concentrations between ca. 2.0 cal kyr BP to present. The high diatom abundance in this interval is coupled with an increase of relative abundance of *Chaetoceros* RS (up to 72%) which are often associated to upwelling fronts (e.g. Abrantes, 1988, 1991). The data on dinoflagellate cyst assemblages and $\delta^{18}O$ of *Neoglobodadrina pachyderma* (s) indicate that in this period the vertical water density gradients decreased and active overturning cells were formed in the basin with the final exhaustion of the Northern Hemisphere ice sheet meltwater supplies (Van Nieuwenhove et al., 2016). The abundance ratios of *Emiliania huxleyi* and *Coccolithus pelagicus* and *Gephyrocapsa muelleriae* indicate that this change was concurrent with an overall increase of Atlantic water flow from 3000 a until present (Dylmer et al., 2013).

Taken together these results may suggest enhanced algal productivity in the Storfjorden area, most likely associated to the vicinity of the Arctic Front. This idea is further supported by the peak of relative abundance of the cold *C. pelagicus* that dominates the surface sediment coccolith assemblages west of the front in the modern Nordic Seas (Baumann et al., 2000). The alkenone-SST reconstruction of both SV-04 and the nearby M23258-2 suggests a cooling trend during the late Holocene. These estimates are in accordance with previous literature in the study region (Martrat et al., 2003; Andersen et al., 2004; Rasmussen et al., 2007; Jessen et al., 2010) that reported a gradual cooling of surface waters during this period, the so-called Cool Late Holocene (Fig. 5; Andersen et al., 2004). This cooling was also concurrent with an extension of the spring sea ice coverage in northern positions of the study site such as the Fram strait (Müller et al., 2012). The driving force behind this late Holocene cooling trend has been related to a slow decrease of summer insolation in polar latitudes of the northern hemisphere (Imbrie et al., 1992; Koç et al., 1993; Wanner et al., 2012); though for the last millennia, this robust cooling trend appears not primarily a response to orbital forcing but arises from a high frequency of explosive volcanism (McGregor et al., 2015).

6. Conclusions

Microfossil (diatom valves, coccoliths and dinocysts), biomarker (alkenones) and quantitative reconstructions of sea surface conditions inferred from the alkenone unsaturation index and the modern analogue technique applied to the dinocyst assemblages on sediment core SV-04 provide new detailed information on the changes in the oceanographic conditions and ice-sheet dynamics in the Storfjorden area (SW Svalbard margin, Arctic Ocean) after LGM. The main conclusions of our study are described as follows:

- Overall, the reconstructions of surface water conditions along core SV-04 are consistent with previous research in the region that highlighted the strong coupling between the advances and retreats of the Svalbard-Barents Sea Ice Sheet, the flow of Atlantic Waters over the Svalbard margin and orbital forcing.
- Inception of deglaciation in the area occurred at about 20 cal kyr BP as recorded in the area by oxidized sediments, although possible ice-sheet thinning and instability already occurred at about 22 cal kyr BP.
- Between 20.6 and 14.6 cal kyr BP the deglaciation of the ice stream grounded at or near the shelf of Storfjorden caused the release and sink of large amounts of meltwater in several episodes that were culminated with the Meltwater Pulse 1A (MWP-1A) of Fairbanks (1989).
- The end of the deglaciation is marked by the onset of the Bølling interstadial at 14.6 cal ka BP coeval with the MWP-1A which termination correspond in the area with a major collapse and retreat of the ice sheet.
- The Allerød warm interstadial is characterized by higher summer SSTs and enhanced biological productivity as a result of the gradually increasing influence of Atlantic waters in Storfjorden.
- Between 12.6 and 11.2 cal kyr BP, the Svalbard-Barents Sea ice sheet retreated into the innermost part of the Barents Sea shelf and fjords resulting in the opening of a sea ice free corridor South of Svalbard that allowed the cold and fresher East Spitsbergen Current to flow in the northernmost Atlantic area. This situation resulted in low winter temperatures, low salinities and enhanced sea-ice cover for up to six months per year.
- Modern-type environmental conditions were rapidly established at the start of the Holocene (11.2 cal kyr BP) at SV-04 site indicating that the Atlantic Waters governed the oceanographic circulation along the Svalbard margin from the early Holocene.
- Reconstructions based on dinocyst data and alkenones indexes at SV-04 suggest relatively warm and stable SSTs between 9.9 and 8.9 kyr BP coinciding with the Holocene Thermal Maximum in the Svalbard region and a decrease in SSTs from 4.2 cal kyr BP to present linked to a decrease of summer insolation in the high latitude northern hemisphere.

Acknowledgement

This study was supported by the Spanish International Polar Year projects SVAIS (POL2006-07390/CGL) and IPY-NICE STREAMS (CTM2009-06370-E). We thank the crew of the BIO Hespérides for their help during the “SVAIS IPY” cruise and José Ignacio Martín Cruz M. Casado, B. Hortelano, Y. Gonzalez-Quinteiro, I. Fernandez for laboratory assistance. A S R-H acknowledges funding from the Junta de Castilla y León (Grupo GR34) and MEC FPU (AP2006-01992). B. M. acknowledges funding from a Ramón y Cajal contract (RYC-2013-14073). We thank K K-H Baumann and an anonymous reviewer for valuable suggestions which have improved the manuscript.

References

- Aagaard, K., Swift, J.H., Carmack, E.C., 1985. Thermohaline circulation in the Arctic Mediterranean Seas. *J. Geophys. Res. Oceans* 90, 4833–4846.

- Aagaard, K., Foldvik, A., Hillman, S.R., 1987. The West Spitsbergen Current: disposition and water mass transformation. *J. Geophys. Res. Oceans* 92, 3778–3784.
- Abrantes, F., 1988. Diatom assemblages as upwelling indicators in surface sediments off Portugal. *Mar. Geol.* 85, 15–39.
- Abrantes, F., 1991. Increased upwelling off Portugal during the last glaciation: diatom evidence. *Mar. Micropaleontol.* 17, 285–310.
- Abrantes, F., Gil, I., Lopes, C., Castro, M., 2005. Quantitative diatom analyses—a faster cleaning procedure. *Deep-Sea Res. I Oceanogr. Res. Pap.* 52, 189–198.
- Alley, R.B., Mayewski, P.A., Sowers, T., Stuiver, M., Taylor, K.C., Clark, P.U., 1997. Holocene climatic instability: a prominent, widespread event 8200 yr ago. *Geology* 25, 483–486.
- Andersen, E.S., Dokken, T.M., Elverhøj, A., Solheim, A., Fossen, I., 1996. Late Quaternary sedimentation and glacial history of the western Svalbard continental margin. *Mar. Geol.* 133, 123–156.
- Andersen, C., Koc, N., Jennings, A., Andrews, J., 2004. Nonuniform response of the major surface currents in the Nordic Seas to insolation forcing: implications for the Holocene climate variability. *Paleoceanography* 19.
- Andersson, C., Pausata, F.S., Jansen, E., Risebrobakken, B., Telford, R.J., 2010. Holocene Trends in the Foraminifer Record from the Norwegian Sea and the North Atlantic Ocean. *Past Climate Variability: Model Analysis and Proxy Intercomparison*.
- Andrulleit, H., 1997. Coccolithophore fluxes in the Norwegian–Greenland Sea: seasonality and assemblage alterations. *Mar. Micropaleontol.* 31, 45–64.
- Andrulleit, H.A., Baumann, K.-H., 1998. History of the last deglaciation and Holocene in the Nordic seas as revealed by coccolithophore assemblages. *Mar. Micropaleontol.* 35, 179–201.
- Assmy, P., Smetacek, V., Montresor, M., Klaas, C., Henjes, J., Strass, V.H., Arrieta, J.M., Bathmann, U., Berg, G.M., Breitbart, E., Cisewski, B., Friedrichs, L., Fuchs, N., Herndl, G.J., Jansen, S., Krägel, S., Latasa, M., Peeken, I., Röttgers, R., Scharek, R., Schüller, S.E., Steigenberger, S., Webb, A., Wolf-Gladrow, D., 2013. Thick-shelled, grazer-protected diatoms decouple ocean carbon and silicon cycles in the iron-limited Antarctic Circumpolar Current. *Proc. Natl. Acad. Sci.* 110, 20633–20638.
- Baeten, N.J., Forwick, M., Vogt, C., Vorren, T.O., 2010. Late Weichselian and Holocene sedimentary environments and glacial activity in Billefjorden, Svalbard. *Geol. Soc. Lond., Spec. Publ.* 344, 207–223.
- Barber, D.C., Dyke, A., Hillaire-Marcel, C., Jennings, A.E., Andrews, J.T., Kerwin, M.W., Bilodeau, G., McNeely, R., Southon, J., Morehead, M.D., Gagnon, J.-M., 1999. Forcing of the cold event of 8200 years ago by catastrophic drainage of Laurentide lakes. *Nature* 400, 344–348.
- Bauch, H.A., Weinelt, M.S., 1997. Surface water changes in the norwegian sea during last deglacial and holocene times. *Quat. Sci. Rev.* 16, 1115–1124.
- Baumann, K.H., Andrulleit, H., Samtleben, C., 2000. Coccolithophores in the Nordic Seas: comparison of living communities with surface sediment assemblages. *Deep-Sea Res. II Top. Stud. Oceanogr.* 47, 1743–1772.
- Berben, S.M.P., Husum, K., Cabedo-Sanz, P., Belt, S.T., 2014. Holocene sub-centennial evolution of Atlantic water inflow and sea ice distribution in the western Barents Sea. *Clim. Past* 10, 181–198.
- Berner, K., Koç, N., Godtliebsen, F., Divine, D., 2011. Holocene climate variability of the Norwegian Atlantic current during high and low solar insolation forcing. *Paleoceanography* 26.
- Birks, C.J.A., Koç, N., 2002. A high-resolution diatom record of late-Quaternary sea-surface temperatures and oceanographic conditions from the eastern Norwegian Sea. *Boreas* 31, 323–344.
- Bischof, J.F., 1994. The decay of the Barents ice sheet as documented in nordic seas ice-rafted debris. *Mar. Geol.* 117, 35–55.
- Bond, G., Showers, W., Cheseby, M., Lotti, R., Almasi, P., deMenocal, P., Priore, P., Cullen, H., Hajdas, I., Bonani, G., 1997. A pervasive millennial-scale cycle in North Atlantic Holocene and glacial climates. *Science* 278, 1257–1266.
- Brassell, S., Eglinton, G., Marlowe, I., Pflaumann, U., Sarnthein, M., 1986. Molecular stratigraphy: a new tool for climatic assessment. *Nature* 320, 129–133.
- Broecker, W.S., Denton, G.H., Edward, R.L., Cheng, H., Alley, R.B., 2010. Putting the Younger Dryas cold event into context. *Quat. Sci. Rev.* 29, 1078–1081.
- Buizert, C., Gkinis, V., Severinghaus, J.P., He, F., Lecavalier, B.S., Kindler, P., Leuenberger, M., Carlson, A.E., Vinther, B., Masson-Delmotte, V., White, J.W.C., Liu, Z., Otto-Bliesner, B., Brook, E.J., 2014. Greenland temperature response to climate forcing during the last deglaciation. *Science* 345, 1177–1180.
- Carbonara, K., Mezgec, K., Varagana, G., Musco, M.E., Lucchi, R.G., Villa, G., Morigi, C., Melis, R., Caffau, M., 2016. Palaeoclimatic changes in Kveithola, Svalbard, during the late Pleistocene deglaciation and Holocene: evidences from microfossil and sedimentary records. *Palaeogeogr. Palaeoclimatol. Palaeoecol.* 463, 136–149.
- Clark, P.U., Mitrovica, J.X., Milne, G.A., Tamisiea, M.E., 2002a. Sea-level fingerprinting as a direct test for the source of global meltwater pulse 1A. *Science* 295, 2438–2441.
- Clark, P.U., Pisias, N.G., Stocker, T.F., Weaver, A.J., 2002b. The role of the thermohaline circulation in abrupt climate change. *Nature* 415, 863–869.
- Clark, P.U., McCabe, A.M., Mix, A.C., Weaver, A.J., 2004. Rapid rise of sea level 19,000 years ago and its global implications. *Science* 304, 1141–1144.
- Condron, A., Winsor, P., 2011. A subtropical fate awaited freshwater discharged from glacial Lake Agassiz. *Geophys. Res. Lett.* 38.
- Cortese, G., Dolven, J.K., Bjørklund, K.R., Malmgren, B.A., 2005. Late Pleistocene–Holocene radiolarian paleotemperatures in the Norwegian Sea based on artificial neural networks. *Palaeogeogr. Palaeoclimatol. Palaeoecol.* 224, 311–332.
- de Vernal, A., Hillaire-Marcel, C., 2000. Sea-ice cover, sea-surface salinity and halo-/thermocline structure of the northern North Atlantic: modern versus full glacial conditions. *Quat. Sci. Rev.* 19, 65–85.
- de Vernal, A., Larouche, A., Richard, P.J.H., 1987. Evaluation of palynomorph concentrations: do the aliquot and the markergrain methods yield comparable results? *Pollen Spores* 29, 291–304.
- de Vernal, A., Guiot, J., Turon, J.-L., 1993. Late and postglacial paleoenvironments of the Gulf of St. Lawrence: marine and terrestrial palynological evidence. *Géog. Phys. Quatern.* 47, 167–180.
- de Vernal, A., Henry, M., Bilodeau, G., 1996a. Techniques de préparation et d'analyse en micropaléontologie. *Les cahiers du GEOTOP. vol. 3 pp.* 16–27.
- de Vernal, A., Hillaire-Marcel, C., Bilodeau, G., 1996b. Reduced meltwater outflow from the Laurentide ice margin during the Younger Dryas. *Nature* 381, 774–777.
- de Vernal, A., Rochon, A., Turon, J.-L., Matthiessen, J., 1997. Organic-walled dinoflagellate cysts: palynological tracers of sea-surface conditions in middle to high latitude marine environments. *Geobios* 30, 905–920.
- de Vernal, A., Hillaire-Marcel, C., Turon, J.-L., Matthiessen, J., 2000. Reconstruction of sea-surface temperature, salinity, and sea-ice cover in the northern North Atlantic during the Last Glacial Maximum based on dinocyst assemblages. *Can. J. Earth Sci.* 37, 725–750.
- de Vernal, A., Eynaud, F., Henry, M., Hillaire-Marcel, C., Londeix, L., Mangin, S., Matthiessen, J., Marret, F., Radi, T., Rochon, A., Solignac, S., Turon, J.L., 2005. Reconstruction of sea-surface conditions at middle to high latitudes of the Northern Hemisphere during the Last Glacial Maximum (LGM) based on dinoflagellate cyst assemblages. *Quat. Sci. Rev.* 24, 897–924.
- de Vernal, A., Hillaire-Marcel, C., Rochon, A., Fréchette, B., Henry, M., Solignac, S., Bonnet, S., 2013. Dinocyst-based reconstructions of sea ice cover concentration during the Holocene in the Arctic Ocean, the northern North Atlantic Ocean and its adjacent seas. *Quat. Sci. Rev.* 79, 111–121.
- Deschamps, P., Durand, N., Bard, E., Hamelin, B., Camoin, G., Thomas, A.L., Henderson, G.M., Okuno, J.i., Yokoyama, Y., 2012. Ice-sheet collapse and sea-level rise at the Bolling warming 14,600[thinsp]years ago. *Nature* 483, 559–564.
- Di, B., Liu, D., Wang, Y., Dong, Z., Li, X., Shi, Y., 2013. Diatom and silicoflagellate assemblages in modern surface sediments associated with human activity: a case study in Sishili Bay, China. *Ecol. Indic.* 24, 23–30.
- Dylmer, C.V., Giraudeau, J., Eynaud, F., Husum, K., De Vernal, A., 2013. Northward advection of Atlantic water in the eastern Nordic Seas over the last 3000 yr. *Clim. Past* 9, 1505–1518.
- Elverhøj, A., Andersen, E.S., Dokken, T., Hebbeln, D., Spielhagen, R., Svendsen, J.I., Sørflaten, M., Rønes, A., Hald, M., Forsberg, C.F., 1995. The growth and decay of the Late Weichselian ice sheet in western Svalbard and adjacent areas based on provenance studies of marine sediments. *Quat. Res.* 44, 303–316.
- Fairbanks, R.G., 1989. A 17,000-year glacio-eustatic sea level record: influence of glacial melting rates on the Younger Dryas event and deep-ocean circulation. *Nature* 342, 637–642.
- Fatela, F., Taborda, R., 2003. Confidence limits of species proportions in microfossil assemblages. *Mar. Micropaleontol.* 45, 169–174.
- Flores, J.A., Sierro, F.J., 1997. A revised technique for the calculation of calcareous nannofossil accumulation rates. *Micropaleontology* 43, 321–324.
- Giraudeau, J., Grelaud, M., Solignac, S., Andrews, J., Moros, M., Jansen, E., 2010. Millennial-scale variability in Atlantic water advection to the Nordic Seas derived from Holocene coccolith concentration records. *Quat. Sci. Rev.* 29, 1276–1287.
- Guiot, J., de Vernal, A., 2011. Is spatial autocorrelation introducing biases in the apparent accuracy of paleoclimatic reconstructions? *Quat. Sci. Rev.* 30, 1965–1972.
- Hald, M., Ebbesen, H., Forwick, M., Godtliebsen, F., Khomenko, L., Korsun, S., Ringstad Olsen, L., Vorren, T.O., 2004. Holocene paleoceanography and glacial history of the West Spitsbergen area, Euro-arctic margin. *Quat. Sci. Rev.* 23, 2075–2088.
- Hald, M., Andersson, C., Ebbesen, H., Jansen, E., Klitgaard-Kristensen, D., Risebrobakken, B., Salomonsen, G.R., Sarnthein, M., Sejrup, H.P., Telford, R.J., 2007. Variations in temperature and extent of Atlantic Water in the northern North Atlantic during the Holocene. *Quat. Sci. Rev.* 26, 3423–3440.
- Hall, I.R., Colmenero-Hidalgo, E., Zahn, R., Peck, V.L., Hemming, S.R., 2011. Centennial- to millennial-scale ice-ocean interactions in the subpolar northeast Atlantic 18–41 kyr ago. *Paleoceanography* 26.
- Hillaire-Marcel, C., de Vernal, A., Piper, D.J.W., 2007. Lake Agassiz Final drainage event in the northwestern North Atlantic. *Geophys. Res. Lett.* 34.
- Hjort, C., Mangerud, J., Adrielsson, L., Bondevik, S., Landvik, J.Y., Salvigsen, O., 1995. Radiocarbon dated common mussels *Mytilus edulis* from eastern Svalbard and the Holocene marine climatic optimum. *Polar Res.* 14, 239–344.
- Hoff, U., Rasmussen, T.L., Stein, R., Ezat, M.M., Fahl, K., 2016. Sea ice and millennial-scale climate variability in the Nordic seas 90[thinsp]kyr ago to present. *Nat. Commun.* 7.
- Imbrie, J., Boyle, E.A., Clemens, S.C., Duffy, A., Howard, W.R., Kukla, G., Kutzbach, J., Martinson, D.G., McIntyre, A., Mix, A.C., Molino, B., Morley, J.J., Peterson, L.C., Pisias, N.G., Prell, W.L., Raymo, M.E., Shackleton, N.J., Toggweiler, J.R., 1992. On the structure and origin of major glaciation cycles 1. Linear responses to Milankovitch forcing. *Paleoceanography* 7, 701–738.
- Ingólfsson, Ó., Landvik, J.Y., 2013. The Svalbard–Barents Sea ice-sheet – historical, current and future perspectives. *Quat. Sci. Rev.* 64, 33–60.
- Jansen, E., Andersson, C., Moros, M., Nisancioglu, K.H., Nyland, B.F., Telford, R.J., 2009. The Early to Mid-Holocene Thermal Optimum in the North Atlantic, Natural Climate Variability and Global Warming. *Wiley Blackwell*, pp. 123–137.
- Jessen, S.P., Rasmussen, T.L., Nielsen, T., Solheim, A., 2010. A new Late Weichselian and Holocene marine chronology for the western Svalbard slope 30,000–0 cal years BP. *Quat. Sci. Rev.* 29, 1301–1312.
- Jordan, R., Stickley, C., 2010. Diatoms as indicators of paleoceanographic events. *The Diatoms: Applications for the Environmental and Earth Sciences*. Cambridge University Press, Cambridge.
- Justwan, A., Koç, N., 2008. A diatom based transfer function for reconstructing sea ice concentrations in the North Atlantic. *Mar. Micropaleontol.* 66, 264–278.
- Kaufman, D.S., Ager, T.A., Anderson, N.J., Anderson, P.M., Andrews, J.T., Bartlein, P.J., Brubaker, L.B., Coats, L.L., Cwynar, L.C., Duvall, M.L., Dyke, A.S., Edwards, M.E., Eisner, W.R., Gajewski, K., Geirsdóttir, A., Hu, F.S., Jennings, A.E., Kaplan, M.R.,

- Kerwin, M.W., Lozhkin, A.V., MacDonald, G.M., Miller, G.H., Mock, C.J., Oswald, W.W., Otto-Bliesner, B.L., Porinchu, D.F., Rühland, K., Smol, J.P., Steig, E.J., Wolfe, B.B., 2004. Holocene thermal maximum in the western Arctic (0–180°W). *Quat. Sci. Rev.* 23, 529–560.
- Kemp, A.E.S., Villareal, T.A., 2013. High diatom production and export in stratified waters – a potential negative feedback to global warming. *Prog. Oceanogr.* 119, 4–23.
- Kemp, A.E.S., Pike, J., Pearce, R.B., Lange, C.B., 2000. The “Fall dump” – a new perspective on the role of a “shade flora” in the annual cycle of diatom production and export flux. *Deep-Sea Res. II Top. Stud. Oceanogr.* 47, 2129–2154.
- Kienast, M., Hanebuth, T.J.J., Pelejero, C., Steinke, S., 2003. Synchronicity of meltwater pulse 1a and the Bølling warming: new evidence from the South China Sea. *Geology* 31, 67–70.
- Klitgaard-Kristensen, D., Sejrup, H.P., Hafliðason, H., Johnsen, S., Spurk, M., 1998. A regional 8200 cal yr BP cooling event in northwest Europe, induced by final stages of the Laurentide ice-sheet deglaciation? *J. Quat. Sci.* 13, 165–169.
- Knutz, P.C., Zahn, R., Hall, I.R., 2007. Centennial-scale variability of the British Ice Sheet: implications for climate forcing and Atlantic meridional overturning circulation during the last deglaciation. *Paleoceanography* 22.
- Koç, N., Jansen, E., Hafliðason, H., 1993. Paleoceanographic reconstructions of surface ocean conditions in the Greenland, Iceland and Norwegian seas through the last 14 ka based on diatoms. *Quat. Sci. Rev.* 12, 115–140.
- Kristensen, D.K., Rasmussen, T.L., Koç, N., 2013. Paleoceanographic changes in the northern Barents Sea during the last 16,000 years—new constraints on the last deglaciation of the Svalbard–Barents Sea Ice Sheet. *Boreas* 42, 798–813.
- Laberg, J.S., Vorren, T.O., 1995. Late Weichselian submarine debris flow deposits on the Bear Island Trough Mouth Fan. *Mar. Geol.* 127, 45–72.
- Łącka, M., Zajączkowski, M., Forwick, M., Szczuciński, W., 2015. Late Weichselian and Holocene palaeoceanography of Storfjordrenna, southern Svalbard. *Clim. Past* 11, 587–603.
- Landvik, J.Y., Bondevik, S., Elverhøi, A., Fjeldskaar, W., Mangerud, J., Salvignen, O., Siegert, J.M., Svendsen, J.J., Vorren, T.O., 1998. The Last Glacial Maximum of Svalbard and the Barents Sea area: ice sheet extent and configuration. *Quat. Sci. Rev.* 17, 43–75.
- Laskar, J., Robutel, P., Joutel, F., Gastineau, M., Correia, A.C.M., Levrard, B., 2004. A long-term numerical solution for the insolation quantities of the Earth. *Astron. Astrophys.* 428, 261–285.
- Liu, Z., Otto-Bliesner, B.L., He, F., Brady, E.C., Tomas, R., Clark, P.U., Carlson, A.E., Lynch-Stieglitz, J., Curry, W., Brook, E., Erickson, D., Jacob, R., Kutzbach, J., Cheng, J., 2009. Transient simulation of last deglaciation with a new mechanism for Bølling-Allerød warming. *Science* 325, 310–314.
- Llopart, J., Urgeles, R., Camerlenghi, A., Lucchi, R.G., Rebesco, M., De Mol, B., 2015. Late Quaternary development of the Storfjorden and Kveithola Trough Mouth Fans, north-western Barents Sea. *Quat. Sci. Rev.* 129, 68–84.
- Loeng, H., 1991. Features of the physical oceanographic conditions of the Barents Sea. *Polar Res.* 10, 5–18.
- Lucchi, R.G., Camerlenghi, A., Rebesco, M., Colmenero-Hidalgo, E., Sierro, F.J., Sagnotti, L., Urgeles, R., Melis, R., Morigi, C., Bárcena, M.A., Giorgetti, G., Villa, G., Persico, D., Flores, J.A., Rigual-Hernández, A.S., Pedrosa, M.T., Macri, P., Caburlotto, A., 2013. Post-glacial sedimentary processes on the Storfjorden and Kveithola trough mouth fans: significance of extreme glacial marine sedimentation. *Glob. Planet. Chang.* 111, 309–326.
- Lucchi, R.G., Sagnotti, L., Camerlenghi, A., Macri, P., Rebesco, M., Pedrosa, M., Giorgetti, G., 2015. Marine sedimentary record of meltwater pulse 1a along the NW Barents Sea continental margin. *Arktos* 1, 1–14.
- Maddison, E.J., Pike, J., Leventer, A., Dunbar, R., Brachfeld, S., Domack, E.W., Manley, P., McClennen, C., 2006. Post-glacial seasonal diatom record of the Mertz Glacier Polynya, East Antarctica. *Mar. Micropaleontol.* 60, 66–88.
- Mangerud, J.A.N., Dokken, T., Hebbeln, D., Heggen, B., Ingólfsson, Ó., Landvik, J.Y., Mejhdahl, V., Svendsen, J.J., Vorren, T.O., 1998. Fluctuations of the Svalbard–Barents Sea Ice Sheet during the last 150,000 years. *Quat. Sci. Rev.* 17, 11–42.
- Martrat, B., Grimalt, J.O., Villanueva, J., van Kreveld, S., Samthein, M., 2003. Climatic dependence of the organic matter contributions in the north eastern Norwegian Sea over the last 15,000 years. *Org. Geochem.* 34, 1057–1070.
- Martrat, B., Jimenez-Amat, P., Zahn, R., Grimalt, J.O., 2014. Similarities and dissimilarities between the last two deglaciations and interglaciations in the North Atlantic region. *Quat. Sci. Rev.* 99, 122–134.
- Massé, G., Rowland, S.J., Sicre, M.-A., Jacob, J., Jansen, E., Belt, S.T., 2008. Abrupt climate changes for Iceland during the last millennium: evidence from high resolution sea ice reconstructions. *Earth Planet. Sci. Lett.* 269, 565–569.
- Matthews, J., 1969. The assessment of a method for the determination of absolute pollen frequencies. *New Phytol.* 68, 161–166.
- Matthiessen, J., Baumann, A., 1997. Dinoflagellate cyst records from the East Greenland continental margin during the last 15,000 years: implications for paleoceanographic reconstructions. In: Hass, C., Kaminski, M. (Eds.), *Micropaleontology and Paleoceanography from the northern North Atlantic* vol. 5. Gryzbowski Foundation Special Publication, pp. 149–165.
- McGregor, H.V., Evans, M.N., Goosse, H., Leduc, G., Martrat, B., Addison, J.A., Mortyn, P.G., Oppo, D.W., Seidenkrantz, M.-S., Sicre, M.-A., Phipps, S.J., Selvaraj, K., Thirumalai, K., Filippson, H.L., Ersek, V., 2015. Robust global ocean cooling trend for the pre-industrial Common Era. *Nat. Geosci.* 8, 671–677.
- McQuoid, M.R., Nordberg, K., 2003. The diatom *Paralia sulcata* as an environmental indicator species in coastal sediments. *Estuar. Shelf Sci.* 56, 339–354.
- Müller, J., Werner, K., Stein, R., Fahl, K., Moros, M., Jansen, E., 2012. Holocene cooling culminates in sea ice oscillations in Fram Strait. *Quat. Sci. Rev.* 47, 1–14.
- Nørgaard-Pedersen, N., Spielhagen, R.F., Erlenkeuser, H., Grootes, P.M., Heinemeier, J., Knies, J., 2003. Arctic Ocean during the Last Glacial Maximum: Atlantic and polar domains of surface water mass distribution and ice cover. *Paleoceanography* 18.
- Ottesen, D., Dowdeswell, J.A., Rise, L., 2005. Submarine landforms and the reconstruction of fast-flowing ice streams within a large Quaternary ice sheet: the 2500-km-long Norwegian-Svalbard margin (57°–80°N). *Geol. Soc. Am. Bull.* 117, 1033–1050.
- Pedrosa, M.T., Camerlenghi, A., De Mol, B., Urgeles, R., Rebesco, M., Lucchi, R.G., 2011. Sea-bed morphology and shallow sedimentary structure of the Storfjorden and Kveithola trough-mouth fans (North West Barents Sea). *Mar. Geol.* 286, 65–81.
- Ragueneau, O., Tréguer, P., Leynaert, A., Anderson, R.F., Brzezinski, M.A., Demaster, D.J., Dugdale, R.C., Dymond, J., Fisher, G., François, R., Heinze, C., Maier-Reimer, E., Martin-Jézéquel, V., Nelson, D.M., Quéguiner, B., 2000. A review of the Si cycle in the modern ocean: recent progress and missing gaps in the application of biogenic opal as a paleoproductivity proxy. *Glob. Planet. Chang.* 26, 317–365.
- Rasmussen, S.O., Andersen, K.K., Svensson, A., Steffensen, J.P., Vinther, B.M., Clausen, H.B., Siggaard-Andersen, M.L., Johnsen, S.J., Larsen, L.B., Dahl-Jensen, D., 2006. A new Greenland ice core chronology for the last glacial termination. *J. Geophys. Res.* Atmos. 111, 2006, 2012, 11.
- Rasmussen, T.L., Thomsen, E., Slubowska, M.A., Jessen, S., Solheim, A., Koç, N., 2007. Paleoceanographic evolution of the SW Svalbard margin (76°N) since 20,000 14C yr BP. *Quat. Res.* 67, 100–114.
- Reimer, P.J., et al., 2009. IntCal09 and Marine09 radiocarbon age calibration curves, 0–50,000 years cal BP. *Radiocarbon* 51, 1111–1150.
- Renssen, H., Seppä, H., Heiri, O., Roche, D.M., Goosse, H., Fichefet, T., 2009. The spatial and temporal complexity of the Holocene thermal maximum. *Nat. Geosci.* 2, 411–414.
- Renssen, H., Seppä, H., Crosta, X., Goosse, H., Roche, D.M., 2012. Global characterization of the Holocene Thermal Maximum. *Quat. Sci. Rev.* 48, 7–19.
- Rigual-Hernández, A.S., Trull, T.W., Bray, S.G., Armand, L.K., 2016. The fate of diatom valves in the Subantarctic and Polar Frontal Zones of the Southern Ocean: sediment trap versus surface sediment assemblages. *Paleoceanogr. Palaeoclimatol. Palaeoecol.* 457, 129–143.
- Rinterknecht, V.R., Clark, P.U., Raisbeck, G.M., Yiou, F., Bitinas, A., Brook, E.J., Marks, L., Zelčs, V., Lunkka, J.-P., Pavlovskaya, I.E., Piotrowski, J.A., Raukas, A., 2006. The last deglaciation of the southeastern sector of the Scandinavian Ice Sheet. *Science* 311, 1449–1452.
- Rochon, A., de Vernal, A., Sejrup, H.-P., Hafliðason, H., 1998. Climatic changes and sea-surface variations during the deglaciation: palynological evidences from the North Sea. *Quat. Res.* 49, 197–207.
- Rochon, A., de Vernal, A., Turon, J.-L., Matthiessen, J., Head, M.J., 1999. Distribution of Recent Dinoflagellate Cysts in Surface Sediments from the North Atlantic Ocean and Adjacent Seas in Relation to Sea-Surface Parameters.
- Rosell-Melé, A., Eglinton, G., Pflaumann, U., Samthein, M., 1995. Atlantic core-top calibration of the U37 K index as a sea-surface palaeotemperature indicator. *Geochim. Cosmochim. Acta* 59, 3099–3107.
- Rosell-Melé, A., Jansen, E., Weinelt, M., 2002. Appraisal of a molecular approach to infer variations in surface ocean freshwater inputs into the North Atlantic during the last glacial. *Glob. Planet. Chang.* 34, 143–152.
- Rüther, D.C., Bjarnadóttir, L.R., Junttila, J., Husum, K., Rasmussen, T.L., Lucchi, R.G., Andreassen, K., 2012. Pattern and timing of the northwestern Barents Sea Ice Sheet deglaciation and indications of episodic Holocene deposition. *Boreas* 41, 494–512.
- Sagnotti, L., Macri, P., Lucchi, R., Rebesco, M., Camerlenghi, A., 2011. A Holocene paleosecular variation record from the northwestern Barents Sea continental margin. *Geochem. Geophys. Geosyst.* 12.
- Saloranta, T.M., Svendsen, H., 2001. Across the Arctic front west of Spitsbergen: high-resolution CTD sections from 1998 to 2000. *Polar Res.* 20, 177–184.
- Salvigsen, O., Forman, S.L., Miller, G.H., 1992. Thermophilous molluscs on Svalbard during the Holocene and their paleoclimatic implications. *Polar Res.* 11, 1–10.
- Samthein, M., Van Kreveld, S., Erlenkeuser, H., Grootes, P., Kucera, M., Pflaumann, U., Schulz, M., 2003. Centennial-to-millennial-scale periodicities of Holocene climate and sediment injections off the western Barents shelf, 75°N. *Boreas* 32, 447–461.
- Schrader, H.J., Gersonde, R., 1978. Diatoms and silicoflagellates. *Utrecht Micropaleontol. Bull.*
- Seidov, D., Antonov, J.I., Arzayus, K.M., Baranova, O.K., Biddle, M., Boyer, T.P., Johnson, D.R., Mishonov, A.V., Paver, C., Zweng, M.M., 2015. Oceanography north of 60°N from World Ocean Database. *Prog. Oceanogr.* 132, 153–173.
- Serreze, M.C., Maslanik, J.A., Scambos, T.A., Fetterer, F., Stroeve, J., Knowles, K., Fowler, C., Drobot, S., Barry, R.G., Haran, T.M., 2003. A record minimum arctic sea ice extent and area in 2002. *Geophys. Res. Lett.* 30.
- Skogseth, R., Haugan, P.M., Jakobsson, M., 2005. Watermass transformations in Storfjorden. *Cont. Shelf Res.* 25, 667–695.
- Ślubowska-Woldengen, M., Koç, N., Rasmussen, T.L., Klitgaard-Kristensen, D., Hald, M., Jennings, A.E., 2008. Time-slice reconstructions of ocean circulation changes on the continental shelf in the Nordic and Barents Seas during the last 16,000 cal yr BP. *Quat. Sci. Rev.* 27, 1476–1492.
- Solignac, S., de Vernal, A., Giraudeau, J., 2008. Comparison of coccolith and dinocyst assemblages in the northern North Atlantic: how well do they relate with surface hydrography? *Mar. Micropaleontol.* 68, 115–135.
- Stabell, B., 1986. A diatom maximum horizon in upper quaternary deposits. *Geol. Rundsch.* 75, 175–184.
- Stroup, J.S., Lowell, T.V., Breckenridge, A., 2013. A model for the demise of large, glacial Lake Ojibway, Ontario and Quebec. *J. Paleolimnol.* 50, 105–121.
- Stuiver, M., Reimer, P.J., 1993. Extended 14C data base and revised Calib 3.0 14C age calibration program. *Radiocarbon* 35, 215–230.
- Taylor, F.J.R., 1987. *The Biology of Dinoflagellates*. Blackwell Scientific Publications.
- Telesiński, M.M., Bauch, H.A., Spielhagen, R.F., Kandiano, E.S., 2015. Evolution of the central Nordic Seas over the last 20 thousand years. *Quat. Sci. Rev.* 121, 98–109.
- Van Nieuwenhov, N., Bauch, H.A., Andruleit, H., 2013. Multiproxy fossil comparison reveals contrasting surface ocean conditions in the western Iceland Sea for the last two interglacials. *Paleoceanogr. Palaeoclimatol. Palaeoecol.* 370, 247–259.

- Van Nieuwenhove, N., Baumann, A., Matthiessen, J., Bonnet, S., de Vernal, A., 2016. Sea surface conditions in the southern Nordic Seas during the Holocene based on dinoflagellate cyst assemblages. *The Holocene* 26, 722–735.
- Villanueva, J., Grimalt, J.O., Labeyrie, L.D., Cortijo, E., Vidal, L., Louis-Turon, J., 1998. Precessional forcing of productivity in the North Atlantic Ocean. *Paleoceanography* 13, 561–571.
- Wanner, H., Solomina, O., Grosjean, M., Ritz, S.P., Jetel, M.t., 2012. Structure and origin of Holocene cold events. *Quat. Sci. Rev.* 30, 3109–3123.
- Weaver, A.J., Saenko, O.A., Clark, P.U., Mitrovica, J.X., 2003. Meltwater pulse 1A from Antarctica as a trigger of the Bølling-Allerød warm interval. *Science* 299, 1709–1713.
- Zamelczyk, K., Rasmussen, T.L., Husum, K., Hafliðason, H., de Vernal, A., Ravna, E.J.K., Hald, M., Hillaire-Marcel, C., 2012. Paleoclimatographic changes and calcium carbonate dissolution in the central Fram Strait during the last 20 ka. *Quat. Res.* 78, 405–416.